Cellulose (2016) 23:1031–1041
DOI 10.1007/s10570-016-0883-4

ORIGINAL PAPER

# Mechanical properties of cellulose nanomaterials studied by contact resonance atomic force microscopy

**Ryan Wagner · Robert J. Moon · Arvind Raman**

Received: 18 September 2015 / Accepted: 8 February 2016 / Published online: 13 February 2016


**Abstract** Quantification of the mechanical properties of cellulose nanomaterials is key to the development of new cellulose nanomaterial based products. Using contact resonance atomic force microscopy we measured and mapped the transverse elastic modulus of three types of cellulosic nanoparticles: tunicate cellulose nanocrystals, wood cellulose nanocrystals, and wood cellulose nanofibrils. These modulus values were calculated with different contact mechanics models exploring the effects of cellulose geometry and thickness on the interpretation of the data. While intra-particle variations in modulus are detected, we did not observe a measureable difference in modulus between the three types of cellulose particles. Improved practices and experimental complications for the characterization of cellulosic nanomaterials with atomic force microscopy are discussed.

**Keywords** Atomic force microscopy · Cellulose nanomaterials · Cellulose nanocrystals · Cellulose nanofibrils · Contact resonance · Nanomechanics



R. Wagner · A. Raman
Birck Nanotechnology Center, Purdue University, West Lafayette, IN 47907, USA
e-mail: raman@purdue.edu

R. Wagner · A. Raman
School of Mechanical Engineering, Purdue University, West Lafayette, IN 47907, USA

R. J. Moon
Forest Products Laboratory, US Forest Service, Madison, WI 53726, USA
e-mail: robertmoon@fs.fed.us

*Present Address:*
R. Wagner (✉)
Material Measurement Laboratory, National Institute of Standards and Technology, Boulder, CO 80305, USA
e-mail: rbwagner187@gmail.com

## Introduction

Cellulose nanomaterials (CNs) have a unique combination of characteristics, such as strong mechanical properties, producibility at industrially relevant quantities, economic feasibility, and low environmental impact. CNs have shown utility in a wide array of applications, suggesting the potential for commercialization across an array of industrial sectors (Hansen et al. 2014; Moon et al. 2011; Siqueira et al. 2010; Samir et al. 2005; Eichhorn 2011; Mariano et al. 2014). Despite this potential there are many barriers hindering commercialization. One of these barriers is the lack of information on the basic properties of different types of CNs (Hansen et al. 2014). The properties, morphology, and dimensions of the CNs are primarily determined by the source of cellulose, type of refinement, and refinement conditions (Moon

et al. 2011; Beck-Candanedo et al. 2005; Elazzouzi-Hafraoui et al. 2008). CNs can generally be classified based on the processing method used for their production. These classes are the chemically processed cellulose nanocrystals (CNCs, 3–20 nm wide, 50–500 nm in length) and the mechanically processed cellulose nanofibrils (CNF, 5–100 nm wide, 500 nm to microns in length).

To help guide the development of commercially relevant CN based products, data on the fundamental properties of CNs is needed. Specifically, this data can be used to validate model predictions of individual CNs, inform multiscale models of CNs, guide the optimization of CN composite properties, and allow for better understanding of manufacturing processes involving CNs. A complication in measuring these properties is that the orientation dependent stacking of cellulose chains within CNs results in material property anisotropy. Studies of the mechanical properties of CNs have investigated the properties in directions relative to the CN fibril longitudinal direction: parallel to it (i.e. axial direction), or perpendicular to it (i.e. transverse direction). The purpose of this paper is to help address the issue of lack of information on basic CN properties by developing improved protocols for characterization CNs.

The elastic properties of CNs have been studied with atomic force microscopy (AFM) (Binnig et al. 1986), Raman spectroscopy, and atomistic simulations. Based on AFM three point bend test measurements (Deng et al. 2009), the axial elastic properties for CN produced from bacteria (Guhados et al. 2005) and tunicate (Iwamoto et al. 2009), were 78 and 145–150 GPa, respectively. Axial elastic properties measurements by Raman spectroscopy reported values of 57–105 GPa for wood based CNCs (Rusli and Eichhorn 2008), 114 GPa for bacterial cellulose (Hsieh et al. 2008), and 143 GPa for tunicate CNCs (Sturcova et al. 2005). Some of the range of reported values is likely to be associated with differences in the experimental techniques or the assumptions used in the model predictions. For example, the difference between reported values for tunicate based CNCs and wood CNCs might be do to the effect of CN aspect ratio on the Raman spectroscopy measurement technique (Rusli and Eichhorn 2008). However, there are indications that cellulose source material and the controlled refinement may influence the axial elastic properties. For example, different dominant crystal structure between bacterial cellulose (Cellulose I$\alpha$) and tunicate cellulose (Cellulose I$\beta$) could influence material properties. The transverse modulus (5–50 GPa) of CNs are less studied, and existing AFM measurements tend to have large uncertainties in the reported values (Wagner et al. 2011). To date the transverse elastic modulus based on force displacement AFM (FZ-AFM) measurements have been reported for CNs derived from wood (Pakzad et al. 2011; Lahiji et al. 2010; Usov et al. 2015), cotton (Pakzad et al. 2011), bacteria (Usov et al. 2015), and tunicate (Wagner et al. 2010, 2011).

The large scatter and uncertainty in the reported elastic constants of CNs makes it difficult to ascertain if there is an effect of the cellulose source or processing on the measured elastic moduli. There is hope that through improved AFM methodologies increased measurement sensitivity can be achieved, making it possible to systematically investigate differences in properties arising from changes of source material and processing technique. Most prior AFM studies of CNs have used a technique called force displacement AFM (FZ-AFM) (Butt et al. 2005). In FZ-AFM the displacement of the sample (Z) is adjusted while the force (F) experienced by the AFM cantilever is recorded. From this force and displacement information, properties of the sample can be inferred. FZ-AFM based techniques work well when indentation of the sample by the AFM tip can be accurately determined from the difference of the sample displacement and cantilever deflection (Wagner et al. 2011). For this to occur the indentation must be significantly greater than the noise floor on both the sample displacement and cantilever deflection channels. This limitation prevents FZ-AFM from accurately characterizing samples that are much stiffer than the AFM cantilever and samples that are very thin, as the maximum achievable indentation in these experiments is too small. The above considerations imply that while FZ-AFM is well suited to the AFM three point bend tests (where the sample can be deformed a large amount) that determine CNs axial modulus, it is poorly suited to measure CNs transverse modulus (where the indentation into the sample is limited by stiffness and thickness). Therefore, applying FZ-AFM to study the transverse properties of CNs has fundamental sensitivity limitations that may prevent it from resolving the small difference elastic properties arising due to differences in cellulose types, sources, and processing.

One approach to overcoming the large uncertainty in FZ-AFM measurements of transverse moduli of CN is to consider methods that exploit the dynamics of the AFM cantilever while interacting with the sample. Such methodologies have the potential for increased measurement sensitivity allowing for small changes in material properties to be resolved. One dynamic AFM method that is particularly well suited for the measurement of stiff nanomaterials at small applied force is contact resonance AFM (CR-AFM) (Rabe et al. 1996). In CR-AFM the cantilever tip is placed in contact with the sample at a constant force, and a resonant vibration of the cantilever is excited. A resonant frequency, or eigenvalue, of the surface-coupled cantilever is then tracked as the cantilever is scanned over the sample. CR-AFM exploits the sensitivity of the resonant frequency, $f$, and quality factor, $Q$, to tip-sample contact stiffness and damping (Rabe et al. 1996). Measurements of $f$ and $Q$ can be related to spring and dashpot boundary conditions in a dynamic Euler–Bernoulli beam model, and a contact mechanics model can then be utilized to determine the elastic and viscoelastic properties of the sample. CR-AFM has been used to measure the nanomechanical properties of a wide variety of material systems (Rabe et al. 2002; Stan et al. 2009; Killgore et al. 2011) and can be adapted to nanomechanical mapping (Yamanaka et al. 2001; Kos et al. 2014; Gannepalli et al. 2011; Kopycinska-Mller et al. 2012). A schematic for a CR-AFM model and CR-AFM experimental result is shown in Fig. 1.

This paper presents experimental results for the transverse elastic modulus measured with CR-AFM on three types of CNs: tunicate CNCs, wood CNCs, and wood CNFs. Wood CNCs and wood CNFs are industrially relevant materials as their production volume can be scaled to industrially relevant quantities. Tunicate CNCs are more of an academic interest as they have a more uniform morphology, lower defects, and higher degree of crystallinity when compared to other types of CNs (Moon et al. 2011). The results of this study are separated into two parts. The first part discusses the methodology development necessary to apply CR-AFM on isolated tunicate CNCs. The second part discusses CR-AFM measurements performed on a sample that has multiple types of CNs (tunicate CNCs, Wood CNCs, and wood CNFs). This result focuses on both the differences between different types of nanoparticles as well as heterogeneities within individual particles. Throughout this paper the authors have attempted to highlight and apply improved experimental practices for characterizing CNs with AFM as compared to the traditional FZ-AFM based approaches used in many of the previous experimental studies.

## Materials and methods

### Contact resonance atomic force microscopy

In order to convert the observed cantilever resonance frequency, $f$, while the cantilever tip is in permanent contact with a sample surface into quantitative material properties two models are needed. A model for the dynamics of the AFM cantilever is needed to relate $f$ to stiffness of the tip-sample contact, $k_s$. A second model

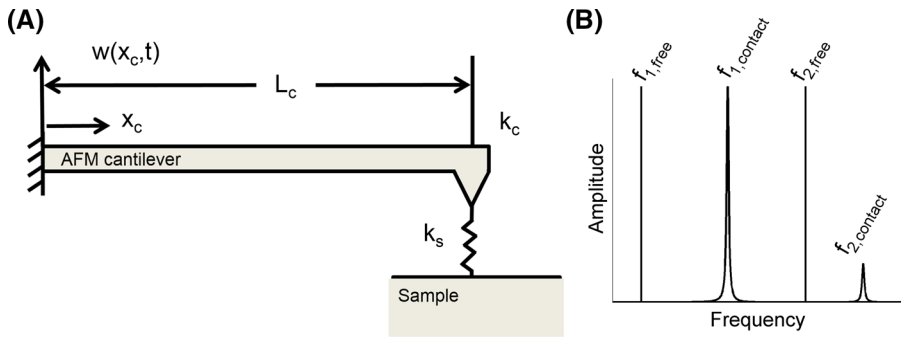


**Fig. 1** **a** Contact resonance AFM experimental schematic. The cantilever of stiffness, $k_c$, and length, $L_c$, is in contact with the sample of stiffness, $k_s$. The deflection of the cantilever is $w(x, t)$, where $x$ is position along the length of the cantilever and $t$ is time. **b** Schematic of typical contact resonance AFM experimental result. When the cantilever is brought into contact and held at a constant average normal force the resonance frequencies ($f_i$) of the cantilever increase. The amount that $f_i$ increases can be used to determine $k_s$, which in tern can be used to determine sample modulus

is needed for the tip-sample interaction force to relate $k_s$ to the elastic modulus of the sample, $E_s$. In CR-AFM theses models are applied in the limit of small cantilever vibration amplitude.

Euler–Bernoulli beam theory relates $f$ to $k_s$ (Rabe et al. 1996). Several different choices for boundary conditions are possible for the Euler–Bernoulli beam equations. We will apply the simple model as shown in Fig. 1a. This model first relates a specific resonance frequency, $f_i$, to a wavenumber, $aL_i$, as: $aL_i = aL_{i,free}\left(\frac{f_i}{f_{i,free}}\right)^{\frac{1}{2}}$, and then relates wavenumber to contact stiffness as:

$$sinh(aL_i)cos(aL_i) - sin(aL_i)cosh(aL_i) = \frac{(aL_i)^3}{3}\frac{k_c}{k_s}(cos(aL_i)cosh(aL_i) + 1). \quad (1)$$

where $k_c$ is the static bending stiffness of the AFM cantilever. Equation 1 is only valid for certain ranges of contact stiffness (Killgore and Hurley 2012), and will typically work best when the dynamic stiffness of the cantilever is comparable to the tip-sample contact stiffness.

Modeling the contact mechanics between the AFM tip and CN is complicated by both the geometry and thickness of the CN. The geometry of the CN is important because it has characteristic length scales that are comparable to the those of the AFM tip. Substrate effects are important because the indentation depth into the CN obtainable with AFM is significant compared to the CN thickness. There does not exist a simple analytical model that can correctly account for both of these effects. Therefore, to investigate these effects we will consider three different contact mechanics models. The Hertz contact mechanics model (Butt et al. 2005) idealizes the tip-sample contact as that of a sphere indenting a semi-infinite elastic half space. This is the most common contact mechanics model used in AFM analysis. The sphere–cylinder contact mechanics model (Stan et al. 2007; Wagner et al. 2011) accounts for sample geometry by modeling the sample as a cylinder. A thin film contact mechanics model (Dimitriadis et al. 2002) introduces a polynomial correction term that accounts for the finite thickness of the sample. We will add an ad-hoc adhesive force to each of these models by following the approach of DMT contact mechanics (Derjaguin et al. 1975) and shifting the entire force versus distance curve down to account for adhesion.

For the cases of the Hertz and sphere–cylinder models we can explicitly write contact stiffness $k$ in terms of the applied force $F$, material properties, and geometric parameters. It is useful to write these equations as $k$ verses force $F$ rather than the more common form of $F$ verses distance $d$ as $k$ and $F$ are directly obtained from the contact resonance AFM experiment whereas $d$ is not. The Hertz contact equation is given as:

$$k = 6^{1/3}(E_{eq})^{2/3}R^{1/3}(F - F_0)^{1/3}, \quad (2)$$

where $F$ is the applied force, $F_0$ is the adhesive force, $R$ is the radius of the AFM tip, and $E_{eq}$ is the equivalent modulus of the tip-sample contact. This version of the Hertz model assumes the sample is a flat semi-infinite half space. The sphere–cylinder contact equation is given as:

$$k = \frac{3}{2}S^{2/3}(E_{eq})^{2/3}\left(\frac{1}{R} + \frac{1}{2R_c}\right)^{-1/3}(F - F_0)^{1/3}, \quad (3)$$

where $R_c$ is the radius of the cylinder, and $S$ is a geometric parameter that must be numerically solved as is discussed elsewhere (Wagner et al. 2011). The sphere–cylinder model assumes that size of the stress field is small relative to the dimensions of the cylinder. For the case of the thin film model $k$ cannot be written explicitly in terms of $F$. The thin film model in terms of $F$ and $d$ is given as:

$$F - F_0 = \frac{4}{3}E_{eq}R^{1/2}d^{3/2}X\left(\frac{\sqrt{Rd}}{h}\right) \quad (4)$$

where $h$ is the thickness of the sample and $X\left(\frac{\sqrt{Rd}}{h}\right)$ is a polynomial function. To proceed Eq. 4 and its derivative $\left(k = \frac{dF}{dd}\right)$ must be solved simultaneously to extract both $d$ and $E_{eq}$. The exact form of $X\left(\frac{\sqrt{Rd}}{h}\right)$ is given elsewhere (Dimitriadis et al. 2002). The thin film model in Eq. 4 assumes that the substrate is rigid. The effect of allowing the substrate to have a finite stiffness can be investigated with alternate thin film models (Hay and Crawford 2011), although this effect is small when compared to difference from the Hertz model. The above models all assume isotropic sample properties.

The equivalent modulus of the tip-sample contact is related to the modulus of the tip and the modulus of the sample in a fashion similar to series springs as:

$$\frac{1}{E_{eq}} = \frac{1-v_s^2}{E_s} + \frac{1-v_t^2}{E_t} \quad (5)$$

where $E_t$ is the modulus of the tip, $E_s$ is the modulus of the sample, $v_t$ is the Poisson's ratio of the tip, and $v_s$ is the Poisson's ratio of the sample.

## Sample preparation

For AFM studies of transverse elasticity the CNs were drop cast onto freshly cleaved, uncoated mica [$M = 53\pm$ 8 GPa (McNeil and Grimsditch 1993; Bobko et al. 2009; Delafargue and Ulm 2004)]. Excess solution was removed with an absorbent material and the sample was blown dry with a nitrogen gun. Three types of CNs are considered in this work: tunicate CNCs, wood CNCs, and wood CNFs. Tunicate and wood refer to the cellulose source. CNCs and CNFs refer to the processing technique: hydrolysis or mechanical processing respectively (Moon et al. 2011). The exact processing conditions the tunicate CNCs, wood CNCs, wood CNFs is described elsewhere (van den Berg et al. 2007; Reiner and Rudie 2013a, b). The density of the CNs on the surface can be controlled by the concentration of the initial solution, the volume of liquid deposited on the surface, and the amount of time the sample is allowed to sit before drying. For the topography images shown in Fig. 2 the details of the sample preparation are 0.1 wt% for the initial CNC solution concentration and 0.01 wt% for the initial CNF concentration, approximately 20 µL drop volume, and approximately 20 s of wait time before drying. Following the approach of Usov et al. (2015), a CN sample containing wood CNC, tunicate CNC, and wood CNF were simultaneously deposited to compare elastic properties. The initial solutions were mixed at a ratio of 1:1:0.1 before deposition. The type of CN can be determined based on the AFM topography image.

## Experimental procedure

AFM experiments were performed on a MFP3D Bio AFM system (Asylum Research) in ambient air at a temperature of about 20 °C and a relative humidity of about 30 %. Cantilever resonances were excited by a broadband, heavily damped piezoelectric transducer mounted beneath the sample (Contact Resonance Sample Actuator, Asylum Research). CONTR cantilevers (Nanosensors, Germany) with a nominal stiffness of 0.5 nN/nm and a nominal length of 450 µm were used. The actual stiffness of the cantilever used in the CR-AFM experiment was determined to be $0.32 \pm 0.02$ nN/nm with the corrected thermal method (Hutter and Bechhoefer 1993; Butt and Jaschke 1995; Proksch et al. 2004). The first six resonance frequencies, $f_{i,free}$, of the freely vibrating cantilever were determined from the thermal spectra to be 15.97, 97.76, 273.5, 536.8, 886.3, and 1324 kHz respectively. The corresponding free wavenumbers from Euler–Bernoulli beam theory are 1.875, 4.694, 7.855, 10.996, 14.1372, and 17.279. The force applied to the samples $F$ during the CR-AFM experiment was $5.0 \pm 0.5$ nN. This corresponds to a maximum indentation of <1 nm.

To create maps of materials properties with CR-AFM a methodology is needed for tracking resonance frequency as the AFM tip is scanned across the sample. Dual AC resonance tracking (DART) (Gannepalli et al. 2011) measures amplitudes $A_1$ and $A_2$ at frequencies $f_i + \Delta f$ and $f_i - \Delta f$ and tracks resonance frequency by adjusting $f_i$ such that $A_1 - A_2 = 0$. It is a common practice to capture data twice in each fast scan line in an AFM image. This results in two measurements of resonance frequency at each point in the scan, the trace frequency $f_{i,t}$ and retrace frequency $f_{i,tr}$.

DART, or any other frequency tracking procedure, will not perfectly track resonance frequencies across a sample because of transients in the frequency tracking feedback loop, contact geometry, and friction. These effects are more prevalent on samples with significant topography gradients, such as CN. Data where the measured resonance frequency is deemed unreliable has been eliminated from the final analysis of material properties. This data elimination was undertaken with respect to three parameters of the frequency tracking procedure: the magnitudes of $A_1$ and $A_2$, the difference between $A_1$ and $A_2$, and the difference between $f_{i,t}$ and $f_{i,tr}$. Specifically, we neglected data points with $A_1 < 1$ or $A_2 < 1$ mV, $\frac{A_1 - A_2}{A_1} > 0.4$, and $|f_{i,r} - f_{i,tr}| > 8$ kHz. A final filtering step to separated the mica data from the CN data is done based on the height of the topography image.

Good sensitivity in CR-AFM is typically obtained when the dynamic stiffness of the AFM cantilever is comparable to the stiffness of the tip-sample contact. However, the average force applied to the sample is

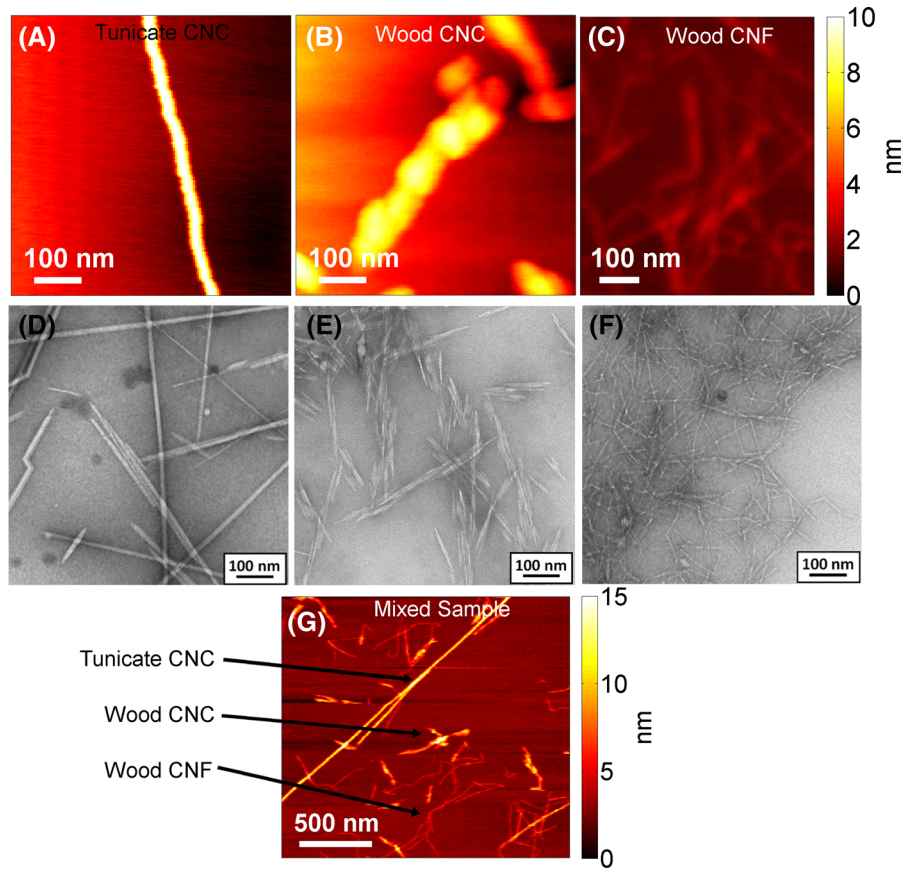


**Fig. 2** Contact mode AFM topography and electron microscopy images of different types of cellulose nanomaterials. **a** Isolated tunicate cellulose nanocrystal sample, **b** isolated Wood cellulose nanocrystal sample, **c** isolated wood cellulose nanofiber sample, **d** electron microscopy image of tunicate cellulose nanocrystals, **e** electron microscopy image of wood cellulose nanocrystals (Reiner and Rudie 2013a), **f** electron microscopy image of wood cellulose nanofibers (Renier and Rudie 2013b). The electron microcopy images are from the same batches of CNs that are studied in this paper. The procedure used for EM imaging is similar to what is describe in Reising et al. (2012). **g** Mixed cellulose nanoparticle sample created from particles shown in **a**–**c**. Based on **a**–**c** it is possible to identify the types of cellulose nanomaterials in **d**

determined by the static stiffness of the AFM cantilever. We have used the higher eigenmode of a softer AFM cantilever (Killgore et al. 2011), specifically the 5th eigenmode, in order to minimize the applied force and maximize material property sensitivity. The 5th eigenmode was chosen because this eigenmode exhibited the maximum absolute and relative frequency shift between the CN and mica substrate.

## Results and discussion

The contact resonance frequency of the 5th CONTR cantilever eigenmode tracked across an isolated individual tunicate CNC is shown in Fig. 3b and the corresponding topography image is shown in Fig. 3a. Using the data filtering process discussed in the "Materials and methods" section the resonance frequency observed on the tunicate CNC was 903.1 ± 4.5 kHz and the resonance frequency observed on surrounding mica was 915.0 ± 2.8 kHz. The error signals used to eliminate data from the final analysis are shown in Fig. 3c–e. Figure 3f shows the stiffness value on the CN and surrounding mica calculated using Eq. 1. The white data points in Fig. 3f are locations where the frequency data has been eliminated from the final analysis based on the data elimination criterion discussed in the "Materials and methods" section.

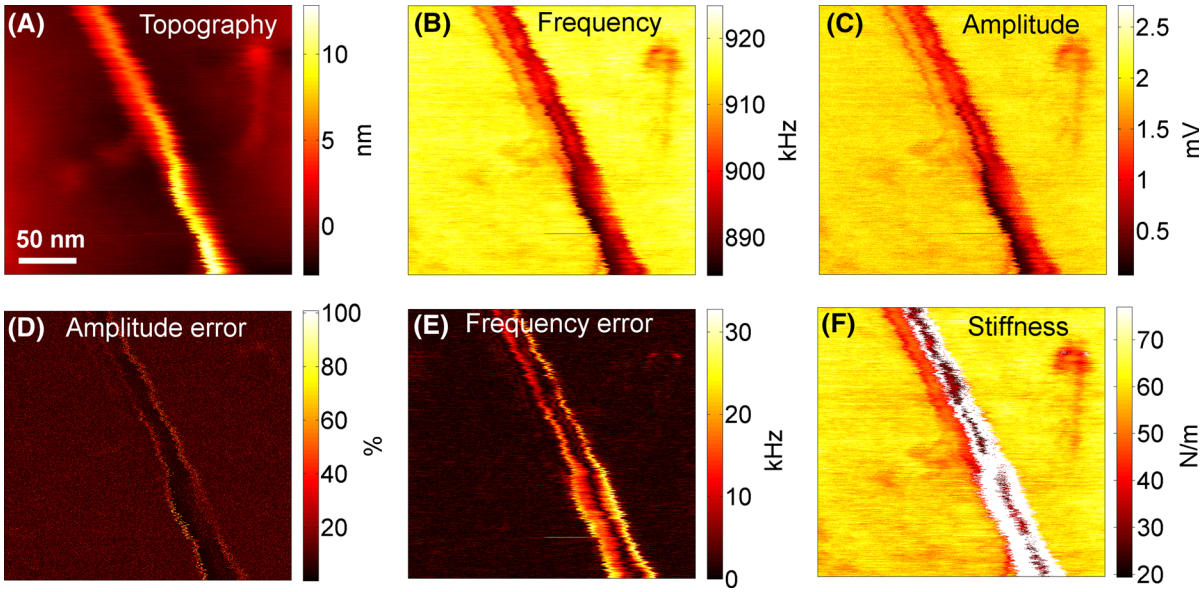


**Fig. 3** AFM contact resonance data on isolated tunicate CNC. **a** Topography image, **b** frequency map, **c** amplitude map, **d** amplitude error map, **e** frequency retrace error map, **f** map of tip-sample contact stiffness. Based on the amplitude map, amplitude error map, and frequency retrace error map some data has been excluded modulus map do to issues with the frequency tracking mechanism. The locations of this excluded data is shown in *white* on the contact stiffness map. The modulus value of the CN is calculated as CN number one in Fig. 6

The stiffness values on the CN shown in Fig. 3f in appear to follow a bimodal distribution. There are two potential explanations for this distribution. It could be an artifact of the AFM measurement arising from the tip-sample geometric convolution, frictional or lateral forces between the tip and sample, or imperfections in the applied frequency tracking procedure. It is also possible that the contrast represents differences in modulus between different crystallographic orientations of the CN. The change in contrast along the length of this CN could correspond to a twist in the CN, thus changing the exposed crystallographic orientation. Twisting of the CN and significant differences in CN modulus in the different transverse crystallographic orientations have been predicted by molecular dynamics simulations of CN (Paavilainen et al. 2011; Dri et al. 2013). Furthermore, 'kinking' of CNs are observed when deposited on mica (Usov et al. 2015). The observed resonance frequency contrast remained consistent with changing scan angle, scan direction, and scan size. However, because of the difficulty in accounting for measurement related artifacts improvements in experimental technique are needed to clearly interpret this contrast.

A sample containing tunicate CNCs, wood CNCs, and wood CNFs was prepared to investigate the effect of CN type on $E_s$ as measured with CR-AFM using the 5th cantilever eigenmode. The advantage of the above experimental design is that the different CNs are measured with the same AFM cantilever, at similar times, and with the exact same experimental conditions. This allows for increased confidence that any observed differences between the particle types is indeed a real effect, and not due to subtle changes in experimental conditions. These results are shown in Fig. 4. Two regions of the mixed sample were selected each containing 2 tunicate CNCs, 2 wood CNCs, and 2 wood CNFs. Tunicate CNC number 1 is the same CN that was shown in Fig. 3.

The measured resonance frequency both on the CNs and mica varies as a function of time. Comparing Fig. 4b–d reveals a difference in average resonance frequency. In Fig. 4b the average resonance frequency 909.6 kHz (yellow on the colorbar) and in Fig. 4d the average resonance frequency is 901.6 kHz (red on the colorbar). A more general analysis of thirty two contact resonance images on the sample shows that there is a consistent decrease in resonance frequency

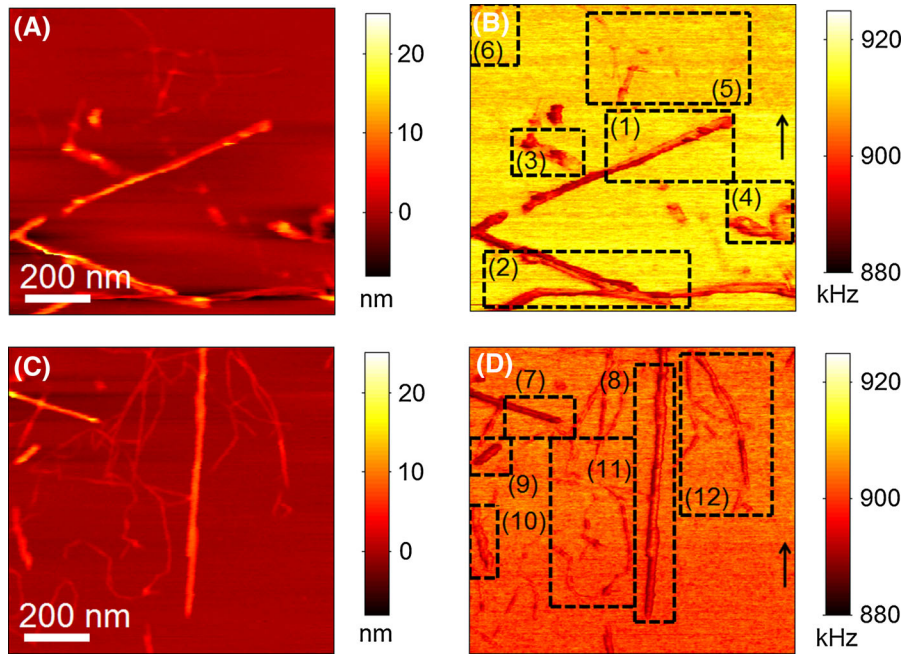


**Fig. 4** AFM contact resonance data on mixed cellulose nanoparticle sample. **a** Topography image of first region, **b** frequency map of the 5th eigenmode of the first region, **c** topography image of second region, **d** frequency map of the 5th eigenmode of the second region. The *numbered boxes* show areas of the sample where data has been extracted for analysis. The *arrows* in **b** and **d** show the location of jumps in resonance frequency in the slow scan direction. (Color figure online)

as a function of time spent scanning. In addition to this longer term drift of resonance frequency, there are also jumps in the resonance frequency in the slow scan direction within a single image.

It is likely that both the slow change over time of resonance frequency and the jumps in resonance frequency are due to contamination of the tip with cellulose. Contamination of the AFM tip with cellulose will result in one of three possible scenarios: (1) the modulus of the tip does not significantly change and the contamination will not effect the experimental results even if the modulus of the tip is neglected in the analysis, (2) the effective modulus of the tip becomes comparable to the modulus of the CN and the contamination will cause the modulus of the CN to be underpredicted if the modulus of the tip is neglected in the analysis, (3) the effective modulus of the tip becomes small relative to the modulus of the CN and the contamination will cause the experiment to be insensitive to the modulus on the CN. We have evaluated the effect of the contamination of the AFM tip with cellulose using the measured resonance frequency on mica and the modulus of mica in the direction of applied force (53 GPa) (McNeil and Grimsditch 1993; Bobko et al. 2009; Delafargue and Ulm 2004). Because the modulus of mica is larger than the modulus of the CN in the direction of the applied force we can conclude that if our experiment is sensitive to the modulus of mica then it is also sensitive to the modulus of the CNs.

To determine if our measurement is sensitive to the modulus of the sample we have computed the equivalent modulus of the tip-sample contact on mica as shown in Fig. 5a, b. These modulus values have been calculated with a $F - F_0$ of 10 nN, an AFM tip radius of 10 nm, a Poisson's ratio for both the tip and sample of 0.3, and in a sample position near the analyzed CN. These values and the known modulus of mica was used to calculate the modulus of the AFM tip for these twelve different cases as shown in Fig. 5c, d. If the modulus of the AFM tip is close to the equivalent modulus of the tip sample contact the measure is insensitive to the modulus of the sample. We will use the metric that the modulus of the AFM tip must be at least 20 % greater than the equivalent modulus of the tip sample contact to avoid this insensitive region. The data in Fig. 4b meets this criteria, while the data in Fig. 4d does not.

Figure 6 shows the modulus values on the CNs from the data set in Fig. 4b calculated with the three different types of contact mechanics models shown in Eqs. 2, 3, and 4. A CN diameter of 8 nm was used for the CNCs and 4 nm for the CNFs. No uncertainty in model parameters was included in the calculation. The

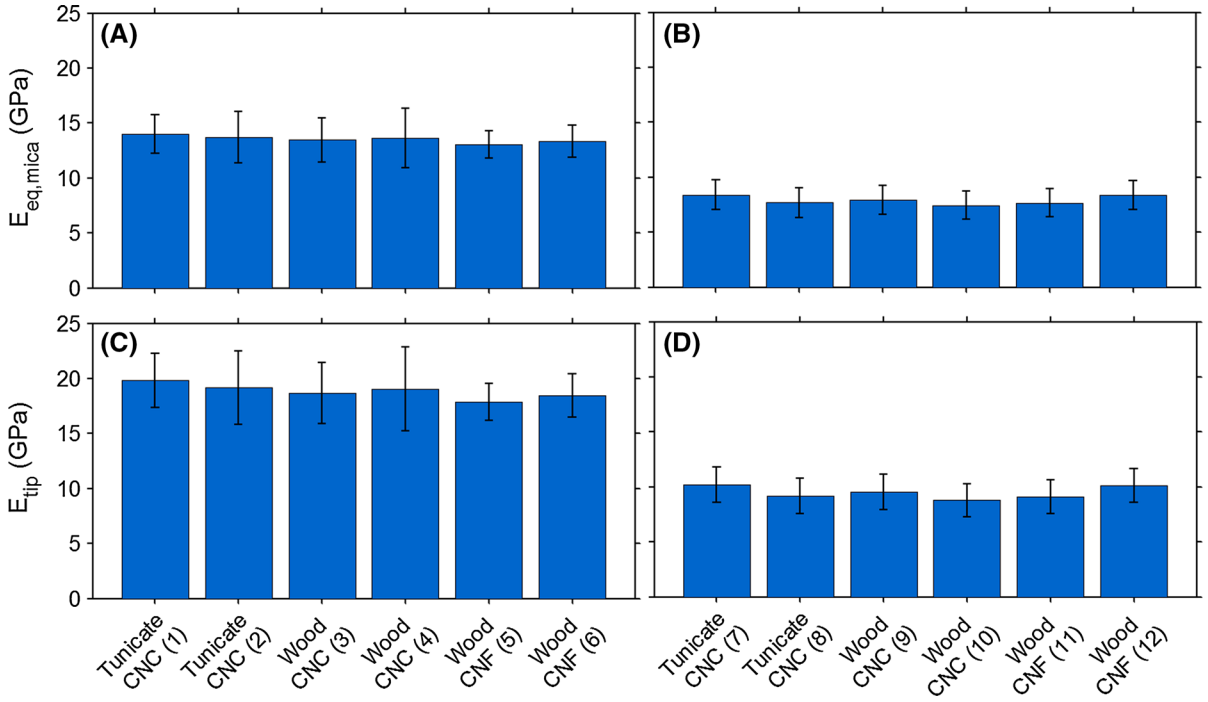


**Fig. 5** Calculated tip modulus values from data in Fig. 4. **a**, **b** Equivalent modulus of the tip-sample contact measured on mica. **c**, **d** AFM tip modulus calculated from the mica data and known modulus of mica. Based on the metric that the equivalent modulus must be 20 % different from the tip modulus to be sensitive to the sample modulus, data sets 7–12 are insensitive to the modulus of the sample due to excessive tip contamination

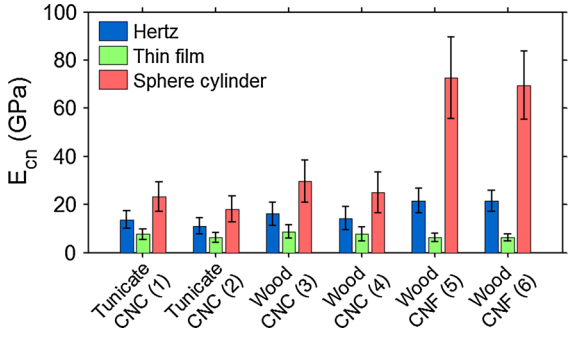


**Fig. 6** Calculated CN modulus values for data sets one through six from Fig. 4b. Three different models are used for data analysis. The modulus of the CN is strongly dependent on the model chosen to analyze the data

given uncertainty bounds only account for variation in measured resonance frequency. It is reasonable to neglect the uncertainties in model parameters when comparing the different CNs we have measured because these uncertainties are largely systematic in nature and thus to not vary over the course of our experiment.

With our technique we did not observe significant difference in modulus between the three types of cellulose nanoparticles analyzed. The crystal to crystal variations within an single type of CN are comparable to the variations between different types of CN. Switching the contact mechanics model from the Hertz based analysis to the thin film based analysis lowers the predicted modulus numbers. The underlying mica substrate causes the Hertz model to appear stiffer than the thin film model on the CN. Switching the contact mechanics model from the Hertz based analysis to the sphere–cylinder based analysis raises the predicted modulus. The smaller contact area caused by the geometry of the tip-sample contact causes the sphere–cylinder model to appear stiffer then the Hertz model. Changing the contact mechanics model away from Hertz has the bigger effect on the smaller diameter CNFs compared to the larger diameter CNCs. The critical model parameters of CN thickness in the thin film model and CN radius in the sphere–cylinder model violate the Hertz model assumptions more drastically as each these parameters

become smaller. Changing the contact mechanics model shifts the sample modulus between 40 and 240 %.

## Conclusions

Using CR-AFM we measured and mapped the transverse elastic modulus of three types of CNs: tunicate CNCs, wood CNCs, and wood CNFs. The transverse elastic moduli were found to be not significantly different from each other and were dependent on the type of contact mechanics model used to interpret the experimental data. Improved practices for characterizing the transverse elastic modulus of CN with AFM have been utilized, specifically: (a) the use of higher eigenmode CR-AFM which maximizes elastic modulus sensitivity while minimizing the maximum applied force and maximum indentation, (b) the elimination of data from the final analysis where it is clear that problems with the CR-AFM frequency tracking procedure are present, and (c) the analysis of multiple types of contact mechanics models. The different contact mechanics models employed accounted for the finite thickness of the CN and the geometry of the CN surface. CR-AFM represents an improvement over FZ-AFM for the characterization of CN because of the ability to limit the maximum indentation into the CN while maintaining measurement sensitivity to mechanical properties. To further improve upon AFM measurements of CNs a more comprehensive effort is needed to model and map the interactions of the AFM tip with the CN. This effort would need to account for the exact indentation geometry of the CN, the interaction with the CN with the underlying substrate, and any nonlinear elastic behavior that arises from complex motion of the individual cellulose chains. This work provides an important step toward the routine, rigorous, and robust characterization of the nanomechanical properties of CNs. A critical aspect in the development of CN based products.

**Acknowledgments** The authors would like to thank the Forest Products laboratory (US Forest Service) Grant No. 12-CR-11111129-076 for funding this research. We are grateful to the Forest Products laboratory for providing the wood CN samples and Professor Christoph Weder (Université de Fribourg) for providing tunicate CN samples. We are also grateful for Jason Killgore (NIST) for helpful discussions regarding the contact resonance AFM technique.

## References

Beck-Candanedo S, Roman M, Gray DG (2005) Effect of reaction conditions on the properties and behavior of wood cellulose nanocrystal suspensions. Biomacromolecules 6(2):1048–1054

Binnig G, Quate C, Gerber C (1986) Atomic force microscope. Phys Rev Lett 56(9):930–933

Bobko CP, Ortega JA, Ulm FJ (2009) Comment on "Elastic modulus and hardness of muscovite and rectorite determined by nanoindentation" by G. Zhang, Z. Wei and R.E. Ferrell [Applied Clay Science 43, (2009) 271–281]. Appl Clay Sci 46(4):425–428

Butt HJ, Jaschke M (1995) Calculation of thermal noise in atomic force microscopy. Nanotechnology 6(1):1–7

Butt HJ, Cappella B, Kappl M (2005) Force measurements with the atomic force microscope: technique, interpretation and applications. Surf Sci Rep 59(1–6):1–152

Delafargue A, Ulm FJ (2004) Explicit approximations of the indentation modulus of elastically orthotropic solids for conical indenters. Int J Solids Struct 41(26):7351–7360

Deng X, Joseph VR, Mai W, Wang ZL, Wu CFJ (2009) Statistical approach to quantifying the elastic deformation of nanomaterials. Proc Natl Acad Sci 106(29):11845–11850

Derjaguin BV, Muller VM, Toporov YP (1975) Effect of contact deformations on the adhesion of particles. J Colloid Interface Sci 53(2):314–326

Dimitriadis EK, Horkay F, Maresca J, Kachar B, Chadwick RS (2002) Determination of elastic moduli of thin layers of soft material using the atomic force microscope. Biophys J 82(5):2798–2810

Dri FL, Hector LG, Moon RJ, Zavattieri PD (2013) Anisotropy of the elastic properties of crystalline cellulose I-beta from first principles density functional theory with Van der Waals interactions. Cellulose 20(6):2703–2718

Eichhorn SJ (2011) Cellulose nanowhiskers: promising materials for advanced applications. Soft Matter 7(2):303–315

Elazzouzi-Hafraoui S, Nishiyama Y, Putaux JL, Heux L, Dubreuil F, Rochas C (2008) The shape and size distribution of crystalline nanoparticles prepared by acid hydrolysis of native cellulose. Biomacromolecules 9(1):57–65

Gannepalli A, Yablon DG, Tsou AH, Proksch R (2011) Mapping nanoscale elasticity and dissipation using dual frequency contact resonance AFM. Nanotechnology 22(35):355705

Guhados G, Wan W, Hutter JL (2005) Measurement of the elastic modulus of single bacterial cellulose fibers using atomic force microscopy. Langmuir 21(14):6642–6646

Hansen F, Brun V, Keller E, Wegner T, Meador M, Friedersdorf L (2014) Cellulose nanomaterials—a path towards commercialization workshop report. http://eprints.internano.org/2224

Hay J, Crawford B (2011) Measuring substrate-independent modulus of thin films. J Mater Res 26(6):727–738

Hsieh YC, Yano H, Nogi M, Eichhorn SJ (2008) An estimation of the young's modulus of bacterial cellulose filaments. Cellulose 15(4):507–513

Hutter JL, Bechhoefer J (1993) Calibration of atomic-force microscope tips. Rev Sci Instrum 64(7):1868–1873

Iwamoto S, Kai W, Isogai A, Iwata T (2009) Elastic modulus of single cellulose microfibrils from tunicate measured by atomic force microscopy. Biomacromolecules 10(9):2571–2576

Killgore JP, Hurley DC (2012) Low force AFM nanomechanics with higher-eigenmode contact resonance spectroscopy. Nanotechnology 23(5):055702

Killgore JP, Kelly JY, Stafford CM, Fasolka MJ, Hurley DC (2011) Quantitative subsurface contact resonance force microscopy of model polymer nanocomposites. Nanotechnology 22(17):175706

Kopycinska-Mller M, Striegler A, Schlegel R, Kuzeyeva N, Khler B, Wolter KJ (2012) Dual resonance excitation system for the contact mode of atomic force microscopy. Rev Sci Instrum 83(4):043703

Kos AB, Killgore JP, Hurley DC (2014) SPRITE: a modern approach to scanning probe contact resonance imaging. Meas Sci Technol 25(2):025405

Lahiji RR, Xu X, Reifenberger R, Raman A, Rudie A, Moon RJ (2010) Atomic force microscopy characterization of cellulose nanocrystals. Langmuir 26(6):4480–4488

Mariano M, Kissi NE, Dufresne A (2014) Cellulose nanocrystals and related nanocomposites: review of some properties and challenges. J Polym Sci Part B Polym Phys 52(12):791–806

McNeil LE, Grimsditch M (1993) Elastic moduli of muscovite mica. J Phys Condens Matter 5(11):1681

Moon R, Martini A, Nairn J, Simonsen J, Youngblood J (2011) Cellulose nanomaterials review: structure, properties, and nanocomposites. Chem Soc Rev 40:3941–3994

Paavilainen S, Róg T, Nairn J, Vattulainen I (2011) Analysis of twisting of cellulose nanofibrils in atomistic molecular dynamics simulations. J Phys Chem B 115(14):3747–3755

Pakzad A, Simonsen J, Heiden PA, Yassar RS (2011) Size effects on the nanomechanical properties of cellulose I nanocrystals. J Mater Res 27(3):528–536

Proksch R, Schffer TE, Cleveland JP, Callahan RC, Viani MB (2004) Finite optical spot size and position corrections in thermal spring constant calibration. Nanotechnology 15(9):1344

Rabe U, Kopycinska M, Hirsekorn S, Saldaa JM, Schneider GA, Arnold W (2002) High-resolution characterization of piezoelectric ceramics by ultrasonic scanning force microscopy techniques. J Phys D Appl Phys 35(20):2621

Rabe U, Janser K, Arnold W (1996) Vibrations of free and surface-coupled atomic force microscope cantilevers: theory and experiment. Rev Sci Instrum 67(9):3281–3293

Reising AR, Moon RJ, Youngblood JP (2012) Effect of particle alignment on mechanical properties of neat cellulose nanocrystal films. J Sci Technol For Prod Process 2(6):32–41

Reiner RS, Rudie AW (2013) Process scale-up of cellulose nanocrystal production to 25 kg per batch at the forest products laboratory. In: Production and applications of cellulose nanomaterials, chapter 1.1. TAPPI Press, pp 21–24

Renier R, Rudie A (2013) Pilot plant scale-up of tempo-pretreated cellulose nanofibrils. In: Production and applications of cellulose nanomaterials, chapter 2.1. TAPPI Press, pp 177–178

Rusli R, Eichhorn SJ (2008) Determination of the stiffness of cellulose nanowhiskers and the fiber-matrix interface in a nanocomposite using Raman spectroscopy. Appl Phys Lett 93(3):033111

Samir MASA, Alloin F, Dufresne A (2005) Review of recent research into cellulosic whiskers, their properties and their application in nanocomposite field. Biomacromolecules 6(2):612–626

Siqueira G, Bras J, Dufresne A (2010) Cellulosic bionanocomposites: a review of preparation, properties and applications. Polymers 2:728–765

Stan G, Ciobanu CV, Parthangal PM, Cook RF (2007) Diameter-dependent radial and tangential elastic moduli of ZnO nanowires. Nano Lett 7(12):3691–3697

Stan G, Ciobanu CV, Thayer TP, Wang GT, Creighton JR, Purushotham KP, Bendersky LA, Cook RF (2009) Elastic moduli of faceted aluminum nitride nanotubes measured by contact resonance atomic force microscopy. Nanotechnology 20(3):035706–035712

Sturcova A, Davies GR, Eichhorn SJ (2005) Elastic modulus and stress-transfer properties of tunicate cellulose whiskers. Biomacromolecules 6(2):1055–1061

Usov I, Nyström G, Adamcik J, Handschin S, Schütz C, Fall A, Bergström L, Mezzenga R (2015) Understanding nanocellulose chirality and structure properties relationship at the single fibril level. Nat Commun 6:7564

van den Berg O, Capadona JR, Weder C (2007) Preparation of homogeneous dispersions of tunicate cellulose whiskers in organic solvents. Biomacromolecules 8(4):1353–1357

Wagner R, Raman A, Moon R (2010) Transverse elasticity of cellulose nanocrystals via atomic force microscopy. In: Proceedings of 10th international conference on wood & biofiber plastic composites, and cellulose nanocomposites symposium. Madison, WI, pp 309–316

Wagner R, Moon R, Pratt J, Shaw G, Raman A (2011) Uncertainty quantification in nanomechanical measurements using the atomic force microscope. Nanotechnology 22(45):455703

Yamanaka K, Maruyama Y, Tsuji T, Nakamoto K (2001) Resonance frequency and Q factor mapping by ultrasonic atomic force microscopy. Appl Phys Lett 78(13):1939–1941